Novel nimesulide multicomponent solid forms: screening, synthesis, thermoanalytical study and characterization

Amanda Cosmo de Almeida[1,2] · Patrícia Osório Ferreira[1] · Maria Vitória Porto[1] · João Canotilho[2,3] ·
Ricardo António Esteves de Castro[2,3] · Flávio Junior Caires[1] · Maria Ermelinda da Silva Eusébio[2]

Abstract

Nimesulide (NMS) is a widely used non-steroidal anti-inflammatory drug, however, presents low aqueous solubility. One way to overcome the solubility issue of drugs is altering their solid forms through some approaches like cocrystals, coamorphous, and eutectic mixtures. The purpose of this work was to prospect new multicomponent solid forms of NMS. A virtual-experimental cocrystal screening was carried out through COSMOquick software and mechanochemical experiments. Alternatively, dual-drug coamorphous systems were investigated by quench cooling and/or cryomilling processes. All solid samples were characterized using differential scanning calorimetry (DSC), powder X-ray diffraction (PXRD) and infrared spectroscopy (FTIR). The results confirmed the successful synthesis of a NMS-piperazine cocrystal (NMS-PPZ), two new eutectic mixtures NMS-gentisic acid (NMS-GSA) and NMS-isoniazid (NMS-INH), as well as novel drug-drug coamorphous systems. The eutectic compositions were determined by binary solid–liquid phase diagram construction and Tamman's triangle plot. Nimesulide-omeprazole (NMS-OMP) coamorphous system was found to be stable for at least 120 days in dry conditions. The coamorphous system with bicalutamide (NMS-BICA) prepared by quench cooling process is more stable than that obtained by cryomilling. Finally, the dissolution rate study demonstrated that NMS multicomponent systems are dissolved relatively faster than pure drug.

Keywords Non-steroidal anti-inflammatory drug · Dual-drug solid systems · Virtual-experimental screening · Thermal analysis · Dissolution rate study

✉ Flávio Junior Caires
flavio.caires@unesp.br

✉ Maria Ermelinda da Silva Eusébio
quierme@ci.uc.pt

Amanda Cosmo de Almeida
amanda.cosmo@unesp.br

Patrícia Osório Ferreira
patricia.osorio@unesp.br

Maria Vitória Porto
mv.porto@unesp.br

João Canotilho
jcano@ci.uc.pt

Ricardo António Esteves de Castro
rcastro@ff.uc.pt

1   School of Sciences, São Paulo State University (Unesp), Bauru, Brazil

2   Chemistry Department, CQC/IMS, University of Coimbra, Coimbra, Portugal

3   Faculty of Pharmacy, University of Coimbra, Coimbra, Portugal

Introduction

Nimesulide (NMS), shown in Fig. 1, is a non-steroidal anti-inflammatory drug (NSAID) that is extensively used worldwide, especially in Brazil, due to its therapeutic properties against pain, fever and inflammation, and also its availability as over-the-counter drug, allowing self-medication [1–3]. Typically, a NMS dosage of 100 mg twice daily is orally administered, but the dose can vary from 100 to 400 mg per day depending on the disorders [4–6]. NMS belongs to the group of NSAIDs that present preferential selective inhibition of the enzyme cyclooxygenase-2 (COX-2), therefore presenting a low incidence of side effects [7, 8]. However, NMS has low aqueous solubility (about 0.01 mg mL^{-1} at 25 °C) [9–11].

The low aqueous solubility of active pharmaceutical ingredients (APIs) compromises the desired plasmatic concentration and, consequently, limits their oral bioavailability and clinical efficacy [12–14]. NMS, as

Fig. 1 Chemical structures of NMS and selected coformers explored in this study

Nimesulide   Piperazine   Gentisic acid   Isoniazid

Omeprazole   Bicalutamide
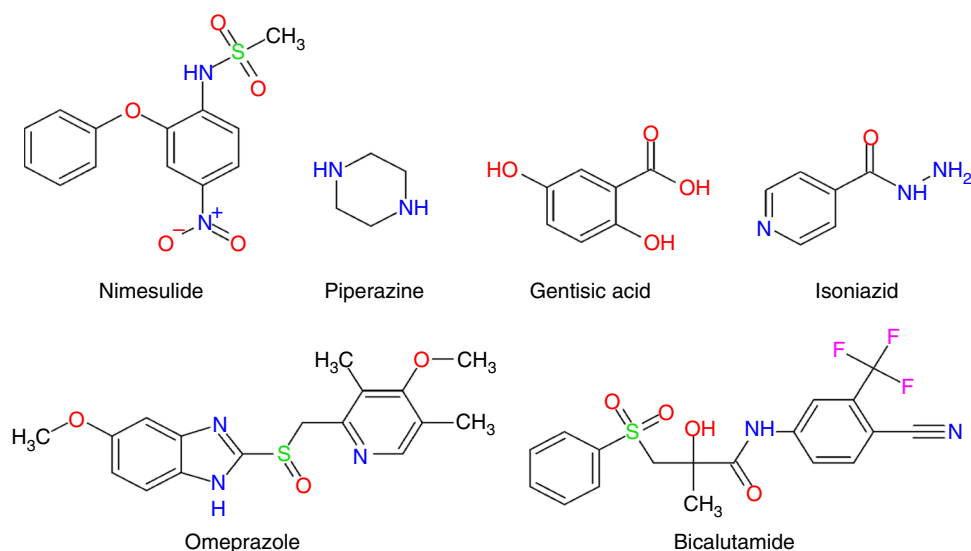
well as other NSAIDs, is categorized as a class II drug in Biopharmaceutical Classification System (BCS), corresponding to those that present high permeability and low aqueous solubility [9–11].

Several strategies have been used to overcome the solubility issue. One of them is the use of multicomponent solid forms, like salts, cocrystals, eutectic mixtures and coamorphous systems, which are capable of altering the physicochemical properties of drugs without affecting the pharmacological ones [15–21]. In the case of dual-drug multicomponent solid forms, in addition to pharmacokinetic improvement, there may be an increase in its activities synergistically, therapeutic combination and/or reduction of side effects [11, 22, 23].

Pharmaceutical cocrystals are multicomponent crystalline forms, in which an API and one or more coformers are linked in a defined stoichiometry by non-covalent and non-ionic intermolecular interactions, such as hydrogen bonding, van der Waals forces and π-π stacking. Commonly, the cocrystal-forming components are neutral and solids at ambient conditions [24–27]. Meanwhile eutectic mixtures comprise two (or more) solids that result in a mixture with lower melting point than the precursors, being miscible in the liquid state and immiscible in the solid state. They maintain the crystal structure of the starting materials [28, 29].

The conversion of a crystalline API to its amorphous phase could achieve an increased solubility and dissolution rate. However, amorphous drugs present higher energy and entropy due to the lack of long-range order, the solid is more unstable than its crystalline counterparts and tends to crystallize over time [30–32]. Alternatively, co-amorphous systems mix small coformers with the API preventing the drug molecules aggregation, therefore increasing the kinetic stability. They are homogeneous multicomponent amorphous phases characterized by a single glass-transition temperature (Tg) and are stabilized by intermolecular interactions and/or mixing effects [10, 32, 33].

Considering that few papers report obtaining of NMS multicomponent solid forms [9, 10, 33–36], the present work focused in prospecting new NMS multicomponent solid systems, using coformers with different functional groups, systematic molecular diversity, and/or with potential for desired therapeutic combination with NMS. A set of 30 coformers was selected, as presented in Table S1. A deeper investigation was performed concerning the coformers piperazine, gentisic acid, isoniazid, omeprazole and bicalutamide, Fig. 1.

Materials and methods

List of chemicals used

A detailed list of all chemicals employed in this study is displayed in Table S1 (supplementary material).

Virtual-experimental cocrystal screening approach

The virtual cocrystal screening of NMS was performed using COSMOquick software (Biovia version 2021, Dassault Systèmes, Germany). The COSMOquick software is a tool based on the COSMO-RS theory, that contains a database of already compiled σ-profiles of several compounds and avoids the time-consuming and costly quantum-chemical calculations [37, 38]. The method calculates the excess enthalpy (ΔH_{excess}) of an undercooled liquid mixture of the components, reflecting the interaction strength of the API and coformer. Another important parameter in the cocrystal

formation prediction is the flexibility parameter (F_{fit}) that combines the molecular interactions (ΔH_{excess}) with the number of rotatable bonds in the molecules [37–39].

A set of 30 coformers was chosen to explore diverse functional groups that could be compatible with NMS ones and/or in a dual-drug perspective (see Table S2, supplementary material), and submitted to the "cocrystal and solvate screening" tool. The SMILES notation, for each compound was employed as input data. The output result generated a list which could be compiled by excess enthalpy (ΔH_{excess}) and flexibility parameter (F_{fit}) [38, 40]. In parallel to the virtual screening, NMS + coformer mixtures were submitted to an experimental cocrystal screening through a mechanochemical approach. Some were also slurried in ethyl acetate and/or acetonitrile as mentioned below.

Mechanochemical synthesis

Equimolar mixtures of starting materials (approximately 100 mg in total) were milled in a MM400 Retsch ball mil (Retsch GmbH & Co., Germany) at an operating frequency of 15 and/or 30 Hz for 30 min. The samples were placed in a 10 mL stainless steel jar with one 7 mm stainless steel ball. A small amount of ethanol ($\eta = 0.25$ μL mg^{-1}) was employed in the liquid-assisted grinding (LAG) process [41]. Some samples were ground in a neat (NG) condition. All the resultant solid products were collected and stored in hermetically sealed containers till further characterization and evaluation.

It is worth pointing out that all the precursors employed in this step of experimental cocrystal screening were submitted to LAG experiments—and subsequently characterized by DSC, PXRD and FTIR techniques—to ensure that this process does not alter their structural characteristics. Furthermore, other binary compositions were prepared at 15 Hz for NMS-GSA and NMS-INH systems and analyzed by DSC.

Slurry

In a first batch, NMS binary equimolar solid mixtures with caffeine (CAF), ciprofloxacin (CIP), norfloxacin (NOR), piperazine (PPZ), theobromine (TBM) and theophylline (THEO) were slurried overnight in ethyl acetate ($\eta = 5$ μL mg^{-1}) [42, 43]. On a second batch, the selected coformers (except PPZ) were slurried with NMS for 72 h in acetonitrile. The wet paste was stirred at 400 rpm using a magnetic stirrer under 25 °C (controlled using a thermostatic bath). After the experiments, all samples were analyzed by PXRD.

Coamorphous preparation

The coamorphous systems preparation was conducted through three different approaches, cryomilling, "cold NG" and/or quench cooling, as detailed bellow.

Cryomilling (Cryo) and "cold NG"

Cryogenic milling experiments were performed using a MM400 Retsch ball mil (Retsch GmbH & Co., Germany), a 10 mL stainless steel jar with two 7 mm stainless steel balls and liquid nitrogen as coolant. The anti-inflammatory NMS and the selected coformers were mixed in a 1–1 molar ratio (100 mg sample in total). The cryo process was conducted at 30 Hz for 4 cooling cycles, with total milling time of 60 min. Each cycle consisted of immersion of the jars containing the mixtures in liquid nitrogen for approximately 2.5 min, followed by milling for 15 min. The samples were collected and stored in a desiccator at room temperature until further characterization and evaluation.

For the NMS-OMP system, additional experiments were carried out that are identified as "cold NG": The jars containing the solid mixture were pre-cooled in the freezer at $T \approx -20$ °C, for 1.5 h prior to milling (30 Hz. 30 min).

Quench cooling (QC)

Quench cooling processes were performed in situ using a PerkinElmer Pyris1 calorimeter (PerkinElmer, USA) with liquid nitrogen cryofill cooling unit. In such analysis, about 2.5 mg of sample was placed in 50 μL aluminum crucibles with perforated lid and submitted to a nitrogen atmosphere (20 mL min^{-1}). An empty similar aluminum pan was used as a reference. The samples were equilibrated at 25 °C and heated until complete melting (with 10 °C min^{-1} heating rate) to erase the solid history of the samples and ensure mixing of components. After melting, the samples were quickly cooled to −35 °C at a cooling rate of 50 °C min^{-1}. The second heating (10 °C min^{-1}) was carried out to analyze the propensity of conversion of the crystalline material into amorphous state, and then, the Tg temperatures were recorded (midpoints of the characteristic baseline step changes). The calorimeter was calibrated with cyclohexane (for gas chromatography), biphenyl (CRM LGC 2610), and indium (Perkin Elmer, $x = 99.99\%$).

Quench cooling scale-up procedure This procedure was performed to obtain enough sample for dissolution rate tests for the NMS-BICA system. An equimolar mixture was heated in a sealed container to complete melting

in an oven (185 °C) and rapidly cooled in an ice bath. Prior to dissolution rate tests, the obtained QC sample was grinded gently using a mortar and pestle, and DSC and PXRD analyses were carried out to ensure complete coamorphization of the mixture.

Characterization

Differential scanning calorimetry (DSC)

Samples grinded at 15 Hz were analyzed through the Mettler Toledo DSC1 Stare System equipment (Mettler Toledo, Switzerland). The solid material was heated at a heating rate of 10 °C min^{-1} from 25 °C until the thermal stability of each sample under synthetic air atmosphere with a flow rate of 50 mL min^{-1}. The sample mass was kept in the range of 2.5 mg and aluminum crucibles (40 μL) with perforated lid was used as reference and sample holder. Additionally, the DSC data of the NMS-GSA and NMS-INH systems were used to construct the binary solid–liquid phase diagrams and Tamman's triangle plot.

The DSC curves from 30 Hz samples were obtained using a PerkinElmer DSC7 calorimeter (PerkinElmer, USA) with an intracooler unit at −20 °C (ethyleneglycol-water, 1:1, V/V) and nitrogen purge (20 mL min^{-1}) at a heating rate $\beta = 10$ °C min^{-1}. Approximately 2.5 mg of sample were sealed in 50 μL aluminum crucibles with a single hole punched in the lid. An empty pan of the same type was employed as a reference.

The instruments were calibrated using an indium metal standard for Mettler Toledo DSC1 and as described by Silva et al. [44] for PerkinElmer DSC7 calorimeter.

Binary solid–liquid phase diagrams and Tamman's triangle construction NMS-GSA and NMS-INH mixtures of different compositions were analyzed by DSC. Through the thermoanalytical data it was possible to construct the binary solid–liquid phase diagram and Tamman's triangle of these systems, which are tools used for eutectic checking composition. The Tamman's triangle was constructed by plotting the eutectics enthalpy correlated to the sample composition, while binary phase diagrams were constructed by taking the *solidus* and *liquidus* temperatures – the onset temperature (T_{onset}) of first DSC melting event and peak temperature (T_{peak}) of second event that corresponds to the complete melting, respectively – of each sample [9, 29, 45, 46]. For several mixtures, for the determination of the eutectic melting enthalpy, deconvolution of the complex melting peaks was carried out using the peak fitting module in the Origin 7 software (version 7.0300, from OriginLab Corporation). A theoretical diagram (represented by calculated *liquidus* temperatures) was estimated using the

Schröder van-Laar equation, that assumes solid-ideal liquid mixture equilibrium [45–48].

Infrared spectroscopy (FTIR)

The FTIR spectra were obtained in the Nicolet 380 IR spectrophotometer (Thermo Scientific, USA), using an accessory of attenuated total reflectance with diamond crystal, in the range of 4000–400 cm^{-1}, resolution of 2 cm^{-1} and 32 scans per spectrum.

Powder X-ray diffraction (PXRD)

The PXRD patterns were obtained using a Rigaku powder X-ray diffractometer (Rigaku, Japan), model MiniFlex 600, using a copper tube providing radiation CuK$_\alpha$, $\lambda = 1.5418$ Å subjected to 40 kV, current of 15 mA. The samples were scanned in a 2θ angle range from 3 to 40°, in continuous scan mode, with a step size of 0.01° and scan speed of 5° min^{-1}. Silicon was used as external calibrator (SRM 640e). The samples were placed in round zero background holders with spin prior to analysis.

Dissolution rate study

The dissolution rate measurements were carried out in triplicate using a rotating disk apparatus (Wood's apparatus) coupled to a Sotax dissolution tester (SOTAX AG, Switzerland). 50 mg of crystalline NMS and selected systems were taken in the dissolution accessory and compressed to a 0.4 cm radius (0.5026 cm^2) stainless-steel disk using a hydraulic press (Specac press) at a pressure of 1.0 ton during 10 s. The accessory was placed in a jar of 900 mL with phosphate buffer pH 7.4 with 2% of tween 80 (v/v) as dissolution media, pre-heated to 37 °C and stirred at 75 rpm. The experimental conditions follow the Brazilian pharmacopeia for nimesulide tablets [49].

NMS concentration was determined from the absorbance measured online in a Lambda 365 PerkinElmer UV–vis spectrophotometer every 5 min at 397 nm. A calibration curve for pure NMS, obtained at this wavelength, was used. Prior to the experiments, the selectivity of NMS determination by this procedure, relatively to the coformers, was evaluated (see Figures S1 and S2, supplementary material, for details). The remaining solids were analyzed by PXRD and no significant phase transition occurred due to the compression and dissolution processes.

Results and discussion

Virtual-experimental cocrystal screening and coformers selection

Only one article reports obtaining NMS cocrystals [36]. In this regard we explored a combined virtual and experimental screening of NMS cocrystals.

The results obtained, using COSMOquick, for cocrystal screening of NMS with the 30 selected compounds, as well as with the coformers tested by Wang et al. [36], are presented in Table S2 (coformers are organized by structural similarities). It is worth reminding that the coformers were chosen in order to have different functional groups, systematic molecular diversity and/or a combination of desired therapeutic action with NMS. According to the COSMOquick software, the more negative the ΔH_{excess} and the lowest the F_{fit} values, the highest the probability of interaction between the precursors [37, 39, 50, 51]. Negative ΔH_{excess} were obtained for all the coformers tested by Wang et al. [36]. Among them, 1,3-bis(4-pyridyl)propane has the highest F_{fit} value and does not give rise to cocrystals. However, as observed in Table S2, the ΔH_{excess} values for most of the coformers were positive or only slightly negative. This data indicates the low tendency of obtaining NMS cocrystals.

Despite in silico indications, all binary NMS mixtures were submitted to an experimental screening through mechanochemical processes. For some coformers, caffeine, ciprofloxacin, norfloxacin, piperazine, theobromine and theophylline, low negative ΔH_{excess} values were obtained, with different F_{fit}. Nimesulide binary systems with these coformers were also slurried in ethyl acetate and/or acetonitrile. Table S2 (supplementary material) summarizes the virtual-experimental screening results. As a result of this combined screening approach, in addition to the already known NMS cocrystals with bipyridyl and its derivatives [36], only a new cocrystal was identified, a NMS-PPZ 1–1 cocrystal (for this system $\Delta H_{excess} = -0.32$; $F_{fit} = 2.7$), as will be shown in the next section.

When positive ΔH_{excess} are obtained the overall experimental results are in agreement with the virtual screening predictions, since cocrystal formation is not expected. For low negative values, as observed for several NMS coformers such as caffeine, theobromine, and ciprofloxacin, the results are not predictable and certainly depend on subtle association factors.
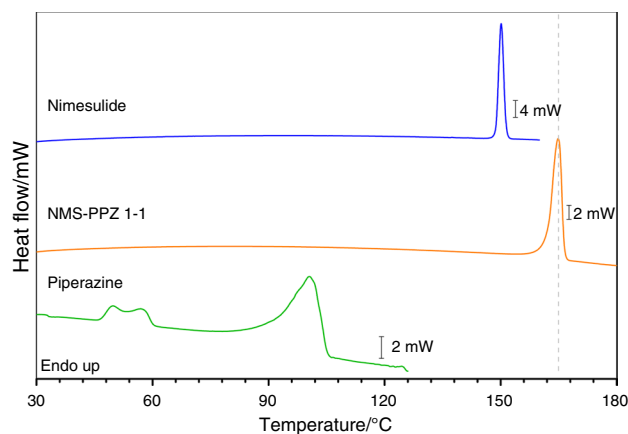

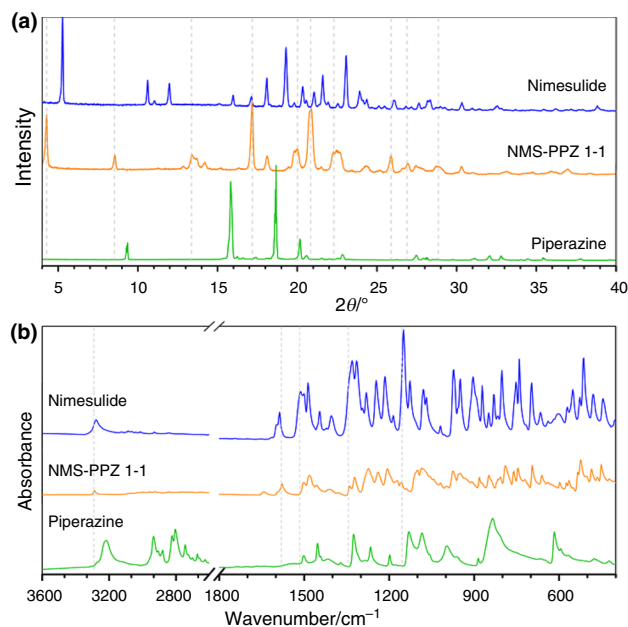**Fig. 2** DSC heating curves of NMS-PPZ equimolar system and pure compounds

Fig. 3 PXRD pattern (**a**) and FTIR spectra (**b**) of NMS-PPZ equimolar system and pure compounds

Nimesulide cocrystals

The DSC data, shown in Fig. 2, gives an unequivocal proof of NMS-PPZ association since the mixture melts above the pure precursors ($T_{onset} = 161.9$ °C; $T_{peak} = 164.9$ °C; $\Delta H = 131.4$ J g^{-1}). Nimesulide presents melting temperature around 149 °C ($T_{onset} = 149.0$ °C; $T_{peak} = 150.5$ °C; $\Delta H = 98.7$ J g^{-1}), while the DSC curve of piperazine presents two endothermic peaks related to water removal and melting/vaporization around 45–60 °C and at 85 °C, respectively [52–55].

The formation of a novel multicomponent solid form is confirmed by PXRD and FTIR analyses, as observed

in Fig. 3a and b, respectively. The diffractograms of raw material correspond to the NMS polymorph form I (CCDC Number: 773602) and PPZ monohydrated form (CCDC Number: 1473720) [52, 56–58]. The NMS-PPZ 1–1 system shows a distinct PXRD pattern when compared to the starting compounds, with new peaks at $2\theta = 4.27°$, 8.56°, 13.38°, 17.17°, 20,01°, 20.87°, 22.31°, 25.88°, 26.94°, 28.86°. Characteristic reflections of the precursors are also absent, as expected.

The FTIR spectrum of pure NMS (Fig. 3b) reveals the main modes of vibration characteristic of N–H stretching at 3277 cm^{-1}, aromatic C=C stretching at 1587 cm^{-1}, N–H bending at 1513 cm^{-1}, symmetric and asymmetric NO$_2$ vibrations at 1318 cm^{-1} and 1501 cm^{-1}, respectively. Furthermore, strong vibrational modes of sulfonyl group appear at 1331 cm^{-1} and 1150 cm^{-1} attributed to asymmetric and symmetric stretching, respectively [9, 59]. The main vibrational bands of PPZ are observed at 3287 cm^{-1} and 1501 cm^{-1} attributed to N–H stretching and bending, respectively [53].

On the other hand, the FTIR spectrum of NMS-PPZ 1–1 system presents evident changes related to the amine and sulfonyl groups. It is possible to verify a decrease of intensity and hypsochromic displacement of the N–H stretching vibrational mode of NMS and PPZ, respectively, from 3277 cm^{-1} and 3216 cm^{-1} to 3287 cm^{-1} in the mixture. Moreover, the symmetrical and asymmetrical stretches of SO$_2$ group are shifted to higher wavenumbers from 1150 cm^{-1} and 1331 cm^{-1} to 1156 cm^{-1} and 1340 cm^{-1}, respectively. The intensity of SO$_2$ bands also decreased [52, 53, 56, 60]. Therefore, the hypsochromic displacements foremost suggest the formation of a new hydrogen bonding network involving NH and SO$_2$ groups, confirming the obtaining of a novel crystal structure. Spectral assignment is summarized in Table S3.

Virtual screening pointed out to NMS-PPZ cocrystal formation, which was confirmed by the experimental results. Since the excess enthalpy (ΔH_{excess}) can be roughly approximated to the free energy of cocrystalization, NMS-PPZ cocrystal formation could be favored [37, 39]. Furthermore, the mechanochemical process can provide mechanical stress, through shear and friction forces, exposing the precursors surface, promoting molecules reorganization and leading to the interaction between NMS and the low molecular-weight coformer PPZ [29, 42]. On the other hand, apart from the good correlation between the virtual and experimental screening of the NMS-PPZ system, the other coformers tested experimentally did not form cocrystals with NMS, as expected. In these cases, the positive or slightly negative ΔH_{excess} values, as well as, the substantially high F_{fit} values indicate low tendency of cocrystallization [37, 39].
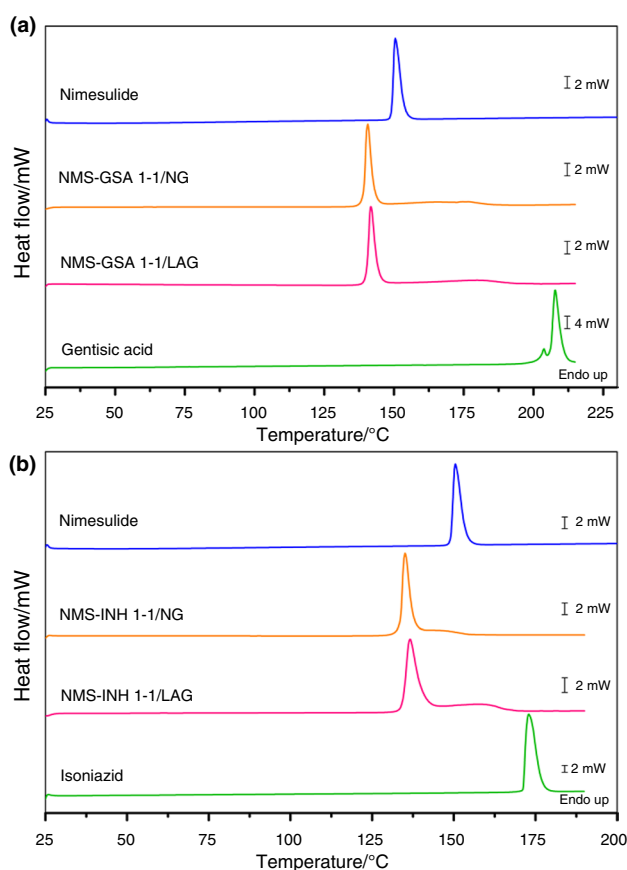

Fig. 4 DSC heating curves of NMS-GSA (**a**) and NMS-INH (**b**) equimolar systems and pure compounds, prepared by NG and by LAG

Nimesulide eutectic mixtures

Gentisic (GSA, or 2,5-dihydroxycarboxylic) acid is a phenolic acid that has been associated as coformer in multicomponent solid approaches since it presents anti-inflammatory, antimicrobial, and antioxidant activities, among others [61, 62]. On the other hand, isoniazid (INH) is an antibiotic drug widely used to treat tuberculosis [63–65]. In this context, NMS-GSA and NMS-INH systems were explored due to their potential for combined therapy.

The DSC curves (Fig. 4a and b) show that NMS-GSA and NMS-INH equimolar samples melt at 138.4 °C and 132.7 °C, respectively, a lower melting temperature than the starting material (NMS at 149.0 °C, GSA at 201.7 °C and INH at 171.0 °C). Infrared spectra and PXRD shown in Figures S3 and S4 for the equimolar samples confirm that they are mixtures of the starting solid precursors.

Both systems show a profile of DSC heating curves, for different compositions, Figs. 5a and 6a that correspond to a typical binary system with a diagram of a simple eutectic. An invariant point—beginning of melting at the

Fig. 5 DSC heating curves (**a**), binary solid–liquid phase diagram (**b**) and Tamman's triangle (**c**) of NMS-GSA system for different compositions. In the phase diagram, the dashed lines, correspond to the prediction of Schröder-van Laar equation [48]
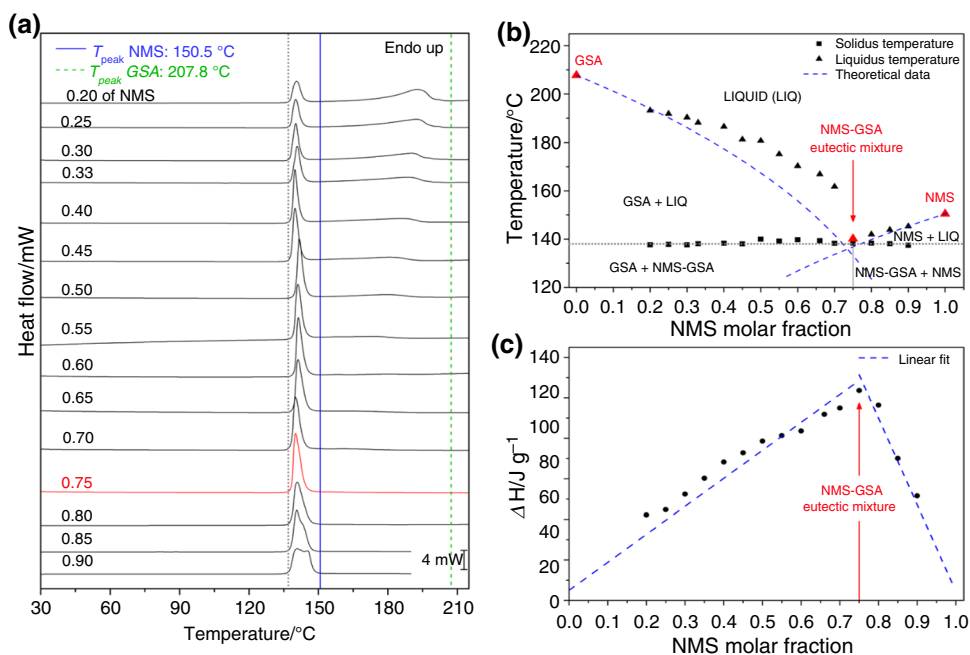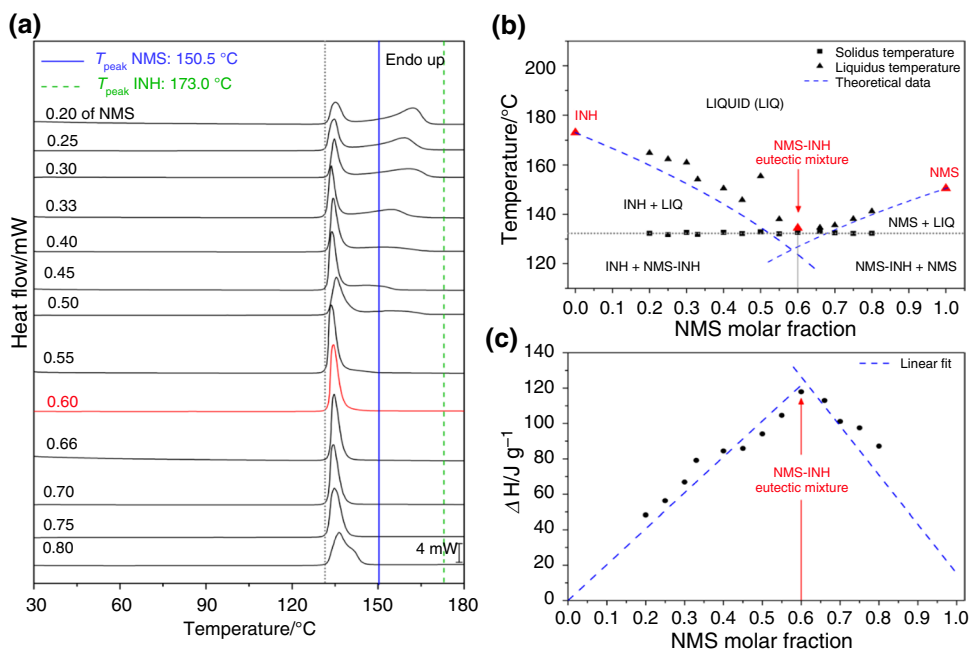

Fig. 6 DSC heating curves (**a**), binary solid–liquid phase diagram (**b**) and Tamman's triangle (**c**) of NMS-INH system for different compositions. In the phase diagram, the dashed lines, correspond to the prediction of Schröder-van Laar equation [48]

same temperature—below the melting of pure compounds is observed at 138 °C to NMS-GSA mixtures and at 132 °C to NMS-INH mixtures [29, 66]. Furthermore, both experimental binary solid–liquid diagrams show some deviation from the respective theoretical diagrams, predicted using the Schröder-van Laar equation, that assumes ideality of the liquid mixtures (Figs. 5b and 6b) [9, 29, 46, 48].

The phase diagrams give an indication of the eutectic compositions that were determined using the Tamman's plots (Figs. 5c and 6c). Tamman's triangle was constructed by plotting the enthalpy of eutectic melting as a function of NMS molar fraction in the mixtures. Therefore, the intersection of the linear fits for hipo and hiper-eutectic compositions pointed out the NMS molar fractions in the eutectic mixture as 0.75 for NMS-GSA and 0.61 for NMS-INH, relative to the mixture with highest enthalpy value [29, 46].

Nimesulide coamorphous systems

Additionally, the present work also explored a coamorphization approach. As mentioned before, a set of APIs were selected focusing on an interesting association with NMS, in a dual-drug perspective. In the literature, only two articles recently report the investigation of NMS coamorphous systems with profen-analogues and indomethacin [10, 33].

Coamorphous systems can be prepared via two different mechanisms, kinetic and thermodynamic disordering processes, such as mechanochemistry and quench cooling, respectively. In mechanochemical methods, the amorphous binary system can be formed directly from the crystalline solid-state by the continuous mechanical stresses. On the other hand, the quenching process involves rapidly cooling the molten sample, a thermodynamically stable non-crystalline form [30, 67].

Equimolar NMS coamorphous systems were investigated through mechanochemistry and/or quench cooling processes. Novel NMS coamorphous systems were obtained with bicalutamide (glass-transition temperature, $Tg = 38$ °C), isoniazid ($Tg = 15$ °C), metoclopramide ($Tg = 39$ °C), p-aminobenzoic acid ($Tg = 19$ °C), piracetam ($Tg = 10$ °C) and omeprazole ($Tg = 32$ °C), as shown in Figure S5 (supplementary material). For amorphous nimesulide the glass-transition temperature is $Tg = 22$ °C, which is in agreement with literature [10, 33]. Some of these equimolar NMS coamorphous mixtures presented glass-transition temperature below that of NMS. Taking this into account, we decided to explore in more detail the NMS-OMP system using different mechanochemical approaches,
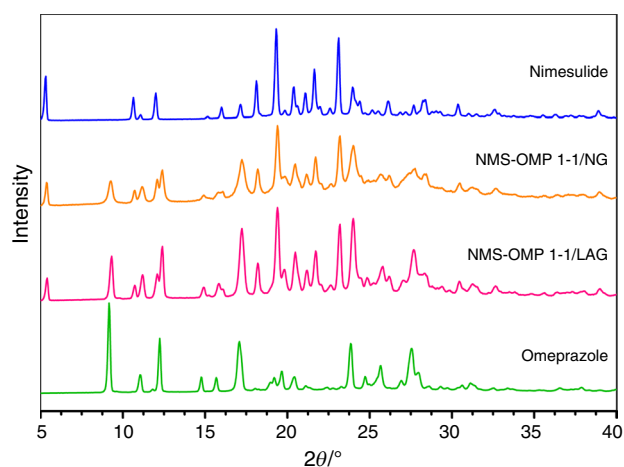

Fig. 8 PXRD pattern of NMS-OMP equimolar mixture and pure compounds, prepared by NG and by LAG

and NMS-BICA system, using both mechanochemistry and quench cooling processes.

Nimesulide–omeprazole system

NMS is a preferential COX-2 inhibitor that can cause gastrointestinal disorders [68, 69]. In this regard, we selected omeprazole (OMP), an anti-acid drug widely used to treat gastric diseases [70, 71], due to the potential of pharmacological association between NMS and OMP.

Previously, into the cocrystal screening process, NMS-OMP equimolar mixture was prepared by mechanochemical method at 15 Hz during 30 min, with or without the addition of ethanol. Regarding the thermal analytical results (Fig. 7)
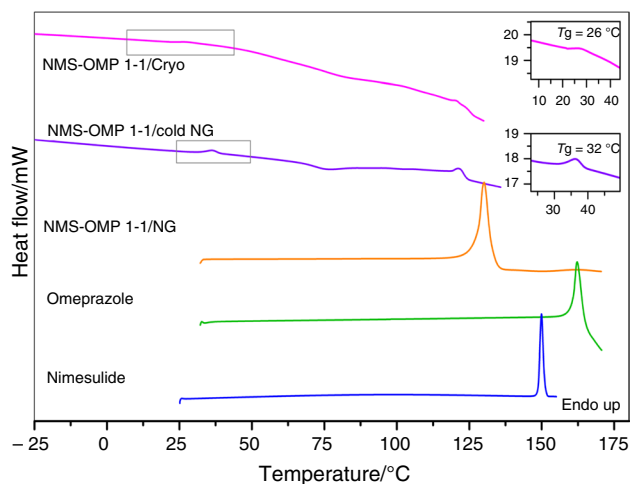

Fig. 7 DSC heating curves of NMS-OMP equimolar mixture and pure compounds, prepared by NG and by LAG

Fig. 9 DSC heating curves of coamorphized NMS-OMP equimolar system and pure compounds

it is observed that both mixtures presented lower melting temperature compared to the isolated APIs.

Complementarily, both PXRD (Fig. 8) and FTIR analyses (Fig. S6, supplementary material) showed a pattern corresponding to the sum of the starting materials profile, indicating that NMS and OMP formed a physical mixture. On the other hand, in the PXRD analysis, it was possible to see a halo of amorphization in the NMS-OMP 1–1/NG sample. Then, in this regard, we performed a trial of coamorphization of this sample. It is worthy mention that coamorphization process was performed exclusively through mechanochemical methods since OMP degrades on melting [72], which makes the quench-cooling approach unfeasible.

Initially, the jars containing the NMS-OMP solid mixture were pre-cooled in the freezer for 1.5 h prior to milling, as described in Sect. 2.3.1. This process was named as "cold NG". Furthermore, the cryomilling process was also performed. These samples were analyzed by DSC, shown in Fig. 9. It is possible to observe a unique Tg event in both DSC curves of NMS-OMP (Cryo) and NMS-OMP (cold NG) at 26 °C and 32 °C, respectively, indicating the coamorphization of samples through these two methodologies [32]. Moreover, during the heating on the DSC analysis, discrete exothermic events around 75 °C can be attributed to crystallization of part of material followed by slight endothermic event around 120 °C, close to melting of NMS-OMP NG physical mixture.

The PXRD of fresh cold NG and cryomilled samples, Fig. 10, show totally amorphized pattern [73]. It is important to highlight that the binary coamorphous systems (stored under dry condition) were periodically analyzed by PXRD. Figure 10 also demonstrates the long-term stability of the coamorphized NMS-OMP systems. It can be inferred that the NMS-OMP cryomilled sample remained totally amorphous for at least 120 days (four months). The material
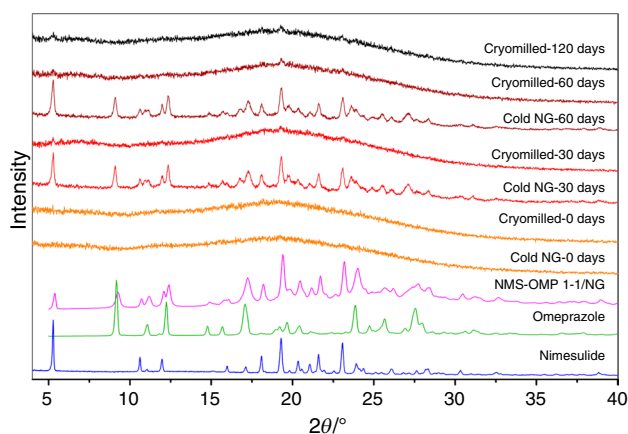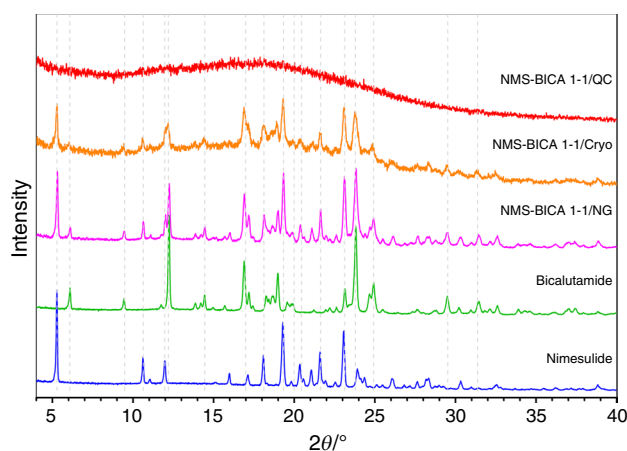

Fig. 11 PXRD pattern of NMS-BICA equimolar mixture and pure compounds

coamorphized through cryomilling was more stable than that obtained by cold NG, since the mixture is cooled much lower than the glass transition temperature, favoring the formation of a disordered phase upon mechanical activation and preventing recrystallization of the sample.
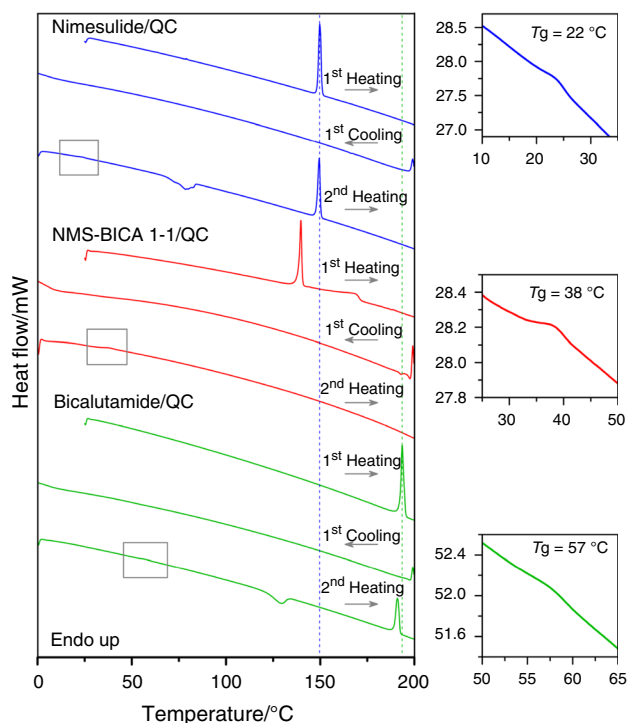

Fig. 10 PXRD pattern of coamorphized NMS-OMP equimolar system and pure compounds

Fig. 12 DSC curves of quench cooled NMS-BICA equimolar mixture and pure compounds

Nimesulide-bicalutamide system

Bicalutamide (BICA) is a non-steroidal antiandrogenic drug used to treat prostate cancer [74, 75], so its association with NMS could be pharmacological interesting. NMS-BICA equimolar mixture was studied through both mechanochemical and quench cooling approaches.

The NMS-BICA sample prepared by NG showed a PXRD pattern (Fig. 11) corresponding to the sum of precursors. Meanwhile, a partial crystalline pattern of Cryo system and a complete amorphous profile for QC sample was observed. In this sense, PXRD results indicate that the quench cooling process is more prone to promoting total crystallinity breakdown [30], being capable to produce a completely amorphous material. Furthermore, the FTIR analysis (Fig. S7) is in agreement with PXRD results: NMS-BICA 1–1 QC system presents broadening of spectral bands, characteristic of amorphous forms and shifting of maxima which indicates the presence of different intermolecular interactions [32, 73, 76].

Concerning to the DSC analysis, Fig. 12, it can be inferred that NMS-BICA 1–1 QC sample presented Tg value (38 °C) intermediate to the quench cooled NMS (22 °C) and BICA (57 °C) [33], and above room temperature. In addition, the NMS-BICA QC coamorphous does not crystallizes during the second heating step, which indicates that this mixture stabilizes the amorphous phase of both drugs.

Dissolution rate study

The dissolution rate tests were performed for pure NMS and three systems, the eutectic samples NMS-INH 3–2 and NMS-GSA 3–1, and the investigated coamorphous system with the highest Tg, NMS-BICA 1–1, an interesting drug-drug association. As shown in Fig. 13, both NMS-BICA 1–1
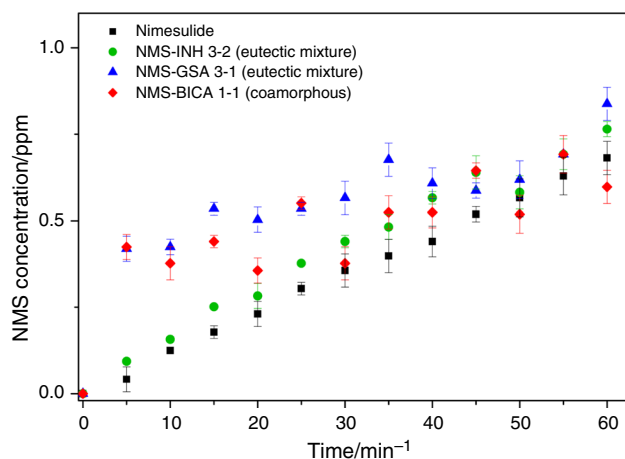

Fig. 13 Dissolution profile of pure NMS and selected multicomponent solid systems

coamorphous system and NMS-GSA 3–1 eutectic mixture presented higher dissolution profiles than the crystalline NMS in the first 25 and 35 min, respectively, while for the NMS-INH 3–2 eutectic mixture only a slight increase is observed. Taking into account the concentration of drug released in 25 min from tablets to the dissolution media, we calculated the increment of NMS released, in percentage, for NMS-BICA coamorphous, for NMS-GSA and NMS-INH eutectic mixtures, relatively to pure nimesulide, that corresponded to 181%, 176% and 124%, respectively.

NMS from these multicomponent systems dissolve faster than the pure drug, with the rate of NMS-BICA ≈ NMS-GSA > NMS-INH > NMS. This results demonstrated that the coamorphous and eutectic systems showed improvement in the dissolution rates, at the initial stage, when compared to the respective original drug, which may favor and accelerate the NMS therapeutic effect [77]. Therefore, these novel multicomponent solid forms may have potential applicability for combined administration with nimesulide, since the three compounds could provide a complementary therapy associated with a non-steroidal anti-inflammatory drug [77].

Conclusions

Using a selected set of coformers, differing in the functional groups and in molecular complexity, both COSMOquick software and mechanochemical approaches point out a low tendency of NMS to form cocrystals. As a result, a novel NMS cocrystal could only be obtained with piperazine, a low molecular weight, simple coformer. Investigation of eutectic mixtures and coamorphous phases was also performed for the coformers with the potential for advantageous therapeutic combination with NMS. Binary solid–liquid phase diagrams and Tamman's triangle plots were constructed for NMS-GSA and NMS-INH systems, and the eutectic compositions determined as 75% and 61% (molar), respectively. Furthermore, several drug-drug coamorphous systems were effectively obtained through the employed methods, the most interesting being NMS-OMP and NMS-BICA. The cryomilled NMS-OMP (1–1) coamorphous solid was stable for at least 120 days in dry conditions. To conclude, dissolution rate tests were performed for NMS-BICA 1–1 coamorphous system, NMS-GSA 3–1 and NMS-INH 3–2 eutectic systems. The comparison of dissolution profiles revealed that, in general, these multicomponent solid systems show higher NMS dissolution rate compared to the pure drug.

References

1. ANVISA. Anuário estatístico do mercado farmacêutico 2022. Brasília; 2023.

2. Macedo LD, Barbosa EJ, Löbenberg R, Bou-Chacra NA. Anti-inflammatory drug nanocrystals: state of art and regulatory perspective. Eur J Pharm Sci. 2021;158:105654. https://doi.org/10.1016/j.ejps.2020.105654.

3. Badri W, Miladi K, Nazari QA, Greige-Gerges H, Fessi H, Elaissari A. Encapsulation of NSAIDs for inflammation management: overview, progress, challenges and prospects. Int J Pharm. 2016;515:757–73. https://doi.org/10.1016/j.ijpharm.2016.11.002.

4. Caiazzo E, Ialenti A, Cicala C. The relatively selective cyclooxygenase-2 inhibitor nimesulide: What's going on? Eur J Pharmacol. 2019;848:105–11. https://doi.org/10.1016/j.ejphar.2019.01.044.

5. Catarro M, Serrano JL, Ramos SS, Silvestre S, Almeida P. Nimesulide analogues: from anti-inflammatory to antitumor agents. Bioorg Chem. 2019;88: 102966. https://doi.org/10.1016/j.bioorg.2019.102966.

6. Ward A, Brogden RN. Nimesulide: a preliminary review of its pharmacological properties and therapeutic efficacy in inflammation and pain states. Drugs. 1988;36:732–53.

7. Güngör T, Ozleyen A, Yılmaz YB, Siyah P, Ay M, Durdağı S, et al. New nimesulide derivatives with amide/sulfonamide moieties: Selective COX-2 inhibition and antitumor effects. Eur J Med Chem. 2021;221: 113566. https://doi.org/10.1016/j.ejmech.2021.113566.

8. Tubić B, Uzunović A, Pilipović S, Gagič Ž. Dissolution profile of nimesulide from pharmaceutical preparations for oral use. Acta Chim Slov. 2016. https://doi.org/10.17344/acsi.2015.2168.

9. Patel RD, Raval MK, Bagathariya AA, Sheth NR. Functionality improvement of Nimesulide by eutectic formation with nicotinamide: exploration using temperature-composition phase diagram. Adv Powder Technol. 2019;30:961–73. https://doi.org/10.1016/j.apt.2019.02.010.

10. Wang M, Liu S, Jia L, Zhang J, Du S, Gong J. Exploring the physical stability of three nimesulide–indomethacin co-amorphous systems from the perspective of molecular aggregates. Eur J Pharm Sci. 2020;147: 105294. https://doi.org/10.1016/j.ejps.2020.105294.

11. Nascimento ALCS, Fernandes RP, Charpentier MD, ter Horst JH, Caires FJ, Chorilli M. Co-crystals of non-steroidal anti-inflammatory drugs (NSAIDs): insight toward formation, methods, and drug enhancement. Particuology. 2021;58:227–41. https://doi.org/10.1016/j.partic.2021.03.015.

12. Blagden N, de Matas M, Gavan PT, York P. Crystal engineering of active pharmaceutical ingredients to improve solubility and dissolution rates. Adv Drug Deliv Rev. 2007;59:617–30. https://doi.org/10.1016/j.addr.2007.05.011.

13. Chadha R, Singh P, Khullar S, Mandal SK. Ciprofloxacin hippurate salt: crystallization tactics, structural aspects, and biopharmaceutical performance. Cryst Growth Des. 2016;16:4960–7. https://doi.org/10.1021/acs.cgd.6b00533.

14. Kotbantao G, Charoenchaitrakool M. Processing of ketoconazole–4-aminobenzoic acid cocrystals using dense CO2 as an antisolvent. J CO2 Util. 2017. https://doi.org/10.1016/j.jcou.2016.12.007.

15. Duggirala NK, Lacasse SM, Zaworotko MJ, Krzyzaniak JF, Arora KK. Pharmaceutical cocrystals: formulation approaches to develop robust drug products. Cryst Growth Des. 2020;20:617–26. https://doi.org/10.1016/j.jcou.2016.12.007.

16. Berry DJ, Steed JW. Pharmaceutical cocrystals, salts and multicomponent systems; intermolecular interactions and property based design. Adv Drug Deliv Rev. 2017;117:3–24. https://doi.org/10.1016/j.addr.2017.03.003.

17. Sathisaran I, Dalvi S. Engineering cocrystals of poorly water-soluble drugs to enhance dissolution in aqueous medium. Pharmaceutics. 2018;10:1–74. https://doi.org/10.3390/pharmaceutics10030108.

18. Uppala S, Vullendula SKA, Yarlagadda DL, Dengale SJ. Exploring the utility of co-amorphous materials to concurrently improve the solubility and permeability of Fexofenadine. J Drug Deliv Sci Technol. 2022;72:103431. https://doi.org/10.1016/j.jddst.2022.103431.

19. Li W, Shi P, Jia L, Zhao Y, Sun B, Zhang M, et al. Eutectics and salt of dapsone with hydroxybenzoic acids: binary phase diagrams. Charact Eval J Pharm Sci. 2020;109:2224–36. https://doi.org/10.1016/j.xphs.2020.04.003.

20. Gopi SP, Banik M, Desiraju GR. New cocrystals of hydrochlorothiazide: optimizing solubility and membrane diffusivity. Cryst Growth Des. 2017;17:308–16. https://doi.org/10.1021/acs.cgd.6b01540.

21. Bolla G, Sanphui P, Nangia A. Solubility advantage of tenoxicam phenolic cocrystals compared to salts. Cryst Growth Des. 2013;13:1988–2003. https://doi.org/10.1021/cg4000457.

22 Bolla G, Nangia A. Pharmaceutical cocrystals: walking the talk. Chem Commun [Internet]. 2016;52:8342–60. https://doi.org/10.1039/C6CC02943D.

23 Li P, Ramaiah T, Zhang M, Zhang Y, Huang Y, Lou B. Two cocrystals of berberine chloride with myricetin and dihydromyricetin: crystal structures, characterization, and antitumor activities. Cryst Growth Des. 2020;20:157–66. https://doi.org/10.1021/acs.cgd.9b00939.

24. Pindelska E, Sokal A, Kolodziejski W. Pharmaceutical cocrystals, salts and polymorphs : advanced characterization techniques. Adv Drug Deliv Rev. 2017;117:111–46. https://doi.org/10.1016/j.ijpharm.2017.03.004.

25. Vishweshwar P, McMahon JA, Bis JA, Zaworotko MJ. Pharmaceutical co-crystals. J Pharm Sci. 2006;95:499–516. https://doi.org/10.1016/j.proche.2014.10.079.

26. Karimi-Jafari M, Padrela L, Walker GM, Croker DM. Creating cocrystals: a review of pharmaceutical cocrystal preparation routes and applications. Cryst Growth Des. 2018;18:6370–87. https://doi.org/10.1021/acs.cgd.8b00933.

27. Qiao N, Li M, Schlindwein W, Malek N, Davies A, Trappitt G. Pharmaceutical cocrystals: an overview. Int J Pharm. 2011;419:1–11. https://doi.org/10.1016/j.ijpharm.2011.07.037.

28. Cherukuvada S, Nangia A. Eutectics as improved pharmaceutical materials: design, properties and characterization. Chem Commun. 2014;50:906–23.

29. Bazzo GC, Pezzini BR, Stulzer HK. Eutectic mixtures as an approach to enhance solubility, dissolution rate and oral bioavailability of poorly water-soluble drugs. Int J Pharm [Internet]. 2020;588:119741. https://doi.org/10.1016/j.ijpharm.2020.119741.

30. Shi Q, Moinuddin SM, Cai T. Advances in coamorphous drug delivery systems. Acta Pharm Sin B. 2019;9:19–35. https://doi.org/10.1016/j.apsb.2018.08.002.

31. Silva JFC, Rosado MTS, Eusébio MES. Structure and energetics of intermolecular association in two lurasidone co-amorphous drug systems. J Mol Struct. 2021;1242: 130709. https://doi.org/10.1016/j.molstruc.2021.130709.

32. Saberi A, Kouhjani M, Yari D, Jahani A, Asare-Addo K, Kamali H, et al. Development, recent advances, and updates in binary, ternary co-amorphous systems, and ternary solid dispersions. J Drug Deliv Sci Technol. 2023;86: 104746. https://doi.org/10.1016/j.jddst.2023.104746.

33. Zhang J, Shi Q, Qu T, Zhou D, Cai T. Crystallization kinetics and molecular dynamics of binary coamorphous systems of nimesulide and profen analogs. Int J Pharm. 2021;610: 121235. https://doi.org/10.1016/j.ijpharm.2021.121235.

34. Georgescu M, Meltzer V, Stănculescu I, Pincu E. Thermal behavior of the nimesulide-salicylic acid eutectic mixtures prepared by mechanosynthesis and recrystallization. Materials (Basel). 2021;14:7715.

35. Abdelkader H, Abdallah OY, Salem H, Alani AWG, Alany RG. Eutectic, monotectic and immiscibility systems of nimesulide with water-soluble carriers: phase equilibria, solid-state characterisation and in-vivo/pharmacodynamic evaluation. J Pharm Pharmacol. 2014;66:1439–50.

36. Wang M, Ma Y, Shi P, Du S, Wu S, Gong J. Similar but not the same: difference in the ability to form cocrystals between nimesulide and the pyridine analogues. Cryst Growth Des. 2021;21:287–96. https://doi.org/10.1021/acs.cgd.0c01132.

37. Kumar A, Nanda A. In-silico methods of cocrystal screening: a review on tools for rational design of pharmaceutical cocrystals. J Drug Deliv Sci Technol. 2021;63: 102527. https://doi.org/10.1016/j.jddst.2021.102527.

38. Loschen C, Klamt A. Solubility prediction, solvate and cocrystal screening as tools for rational crystal engineering. J Pharm Pharmacol. 2015;67:803–11.

39. Guidetti M, Hilfiker R, Kuentz M, Bauer-Brandl A, Blatter F. Exploring the cocrystal landscape of posaconazole by combining high-throughput screening experimentation with computational chemistry. Cryst Growth Des. 2023;23:842–52. https://doi.org/10.1021/acs.cgd.2c01072.

40. Loschen C, Klamt A. COSMOquick : a novel interface for fast σ-profile composition and its application to COSMO-RS solvent screening using multiple reference solvents. Ind Eng Chem Res. 2012;51:14303–8. https://doi.org/10.1021/ie3023675.

41. Friščić T, Childs SL, Rizvi SAA, Jones W. The role of solvent in mechanochemical and sonochemical cocrystal formation: a solubility-based approach for predicting cocrystallisation outcome. Cryst EngComm. 2009;11:418–26. https://doi.org/10.1039/B815174A.

42. Friščič T, Jones W. Recent advances in understanding the mechanism of cocrystal formation via grinding. Cryst Growth Des. 2009;9:1621–37. https://doi.org/10.1021/cg800764n.

43. Friščić T, Mottillo C, Titi HM. Mechanochemistry for synthesis. Angew Chemie: Int Ed. 2020;59:1018–29. https://doi.org/10.1002/anie.201906755.

44. Silva JFC, Pereira Silva PS, Ramos Silva M, Fantechi E, Chelazzi L, Ciattini S, et al. Amorphous solid forms of ranolazine and tryptophan and their relaxation to metastable polymorphs. Cryst Growth Des. 2023;23:6679–91. https://doi.org/10.1021/acs.cgd.3c00565.

45. Lorenz H, Seidel-Morgenstern A. Binary and ternary phase diagrams of two enantiomers in solvent systems. Thermochim Acta. 2002;382:129–42. https://doi.org/10.1016/S0040-6031(01)00746-8.

46. Agafonova EV, Moshchenskiy YV, Tkachenko ML. DSC study and calculation of metronidazole and clarithromycin thermodynamic melting parameters for individual substances and for eutectic mixture. Thermochim Acta. 2014;580:1–6. https://doi.org/10.1016/j.tca.2014.01.018.

47. Ivashenko AV, Titov VV, Kovshev EI. Liquid crystalline compounds: iii on applicability of Schröder-Van Laar equations to liquid crystals mixtures. Mol Cryst Liq Cryst. 1976;33:195–200. https://doi.org/10.1080/15421407608084295.

48. Prigogine I, Defay R. Chemical thermodynamics. Glasgow: Longmans; 1954.

49. ANVISA. Farmacopeia Brasileira, 6a edição. Brasília; 2019 p. 1–1512.

50 Bolla G, Sarma B, Nangia AK. Crystal engineering of pharmaceutical cocrystals in the discovery and development of improved drugs. Chem Rev. 2022;122:11514–603. https://doi.org/10.1021/acs.chemrev.1c00987.

51. Pantwalawalkar J, More H, Bhange D, Patil U, Jadhav N. Novel curcumin ascorbic acid cocrystal for improved solubility. J Drug Deliv Sci Technol. 2021;61:102233. https://doi.org/10.1016/j.jddst.2020.102233.

52. Zhang YX, Wang LY, Dai JK, Liu F, Li YT, Wu ZY, et al. The comparative study of cocrystal/salt in simultaneously improving solubility and permeability of acetazolamide. J Mol Struct. 2019;1184:225–32. https://doi.org/10.1016/j.molstruc.2019.01.090.

53. Moisescu-Goia C, Muresan-Pop M, Simon V. New solid state forms of antineoplastic 5-fluorouracil with anthelmintic piperazine. J Mol Struct. 2017;1150:37–43. https://doi.org/10.1016/j.molstruc.2017.08.076.

54. Bishnoi S, Rochelle GT. Thermodynamics of piperazine/methyldiethanolamine/water/carbon dioxide. Ind Eng Chem Res. 2002;41:604–12. https://doi.org/10.1021/ie0103106.

55 Gálico DA, Perpétuo GL, Castro RAE, Treu-Filho O, Legendre AO, Galhiane MS, et al. Thermoanalytical study of nimesulide and their recrystallization products obtained from solutions of

several alcohols. J Therm Anal Calorim. 2014;115:2385–90. https://doi.org/10.1007/s10973-013-3294-x.

56. Wang N, Huang X, Chen L, Yang J, Li X, Ma J, et al. Consistency and variability of cocrystals containing positional isomers: the self-assembly evolution mechanism of supramolecular synthons of cresol-piperazine. IUCrJ. 2019;6:1064–73. https://doi.org/10.1107/S2052252519012363.

57. Bergese P, Bontempi E, Colombo I, Gervasoni D, Depero LE. Microstructural investigation of nimesulide-crospovidone composites by X-ray diffraction and thermal analysis. Compos Sci Technol. 2003;63:1197–201.

58. Barrio M, Huguet J, Robert B, Rietveld IB, Céolin R, Tamarit JL. Pressure-temperature phase diagram of the dimorphism of the anti-inflammatory drug nimesulide. Int J Pharm. 2017;525:54–9. https://doi.org/10.1016/j.ijpharm.2017.04.016.

59. Nunes JHB, De Paiva REF, Cuin A, Da Costa Ferreira AM, Lustri WR, Corbi PP. Synthesis, spectroscopic characterization, crystallographic studies and antibacterial assays of new copper(II) complexes with sulfathiazole and nimesulide. J Mol Struct. 2016;1112:14–20. https://doi.org/10.1016/j.molstruc.2016.02.006.

60. Bolla G, Mittapalli S, Nangia A. Modularity and three-dimensional isostructurality of novel synthons in sulfonamide-lactam cocrystals. IUCrJ Int Union Crystallogr. 2015;2:389–401. https://doi.org/10.1107/S2052252515004960.

61. Mashhadi SMA, Batsanov AS, Sajjad SA, Nazir Y, Bhatti MH, Yunus U. Isoniazid-gentisic acid cocrystallization: solubility, stability, dissolution rate, antioxidant and flowability properties studies. J Mol Struct. 2021;1226:129388. https://doi.org/10.1016/j.molstruc.2020.129388.

62. Sokal A, Pindelska E, Szeleszczuk L, Kolodziejski W. Pharmaceutical properties of two ethenzamide-gentisic acid cocrystal polymorphs: drug release profiles, spectroscopic studies and theoretical calculations. Int J Pharm. 2017;522:80–9. https://doi.org/10.1016/j.ijpharm.2017.03.004.

63. Cherukuvada S, Nangia A. Fast dissolving eutectic compositions of two anti-tubercular drugs. CrystEngComm. 2012;14:2579.

64. Diniz LF, Souza MS, Carvalho PS, Correa CC, Ellena J. Modulating the water solubility and thermal stability of the anti-tuberculosis drug Isoniazid via multicomponent crystal formation. J Mol Struct. 2018;1171:223–32.

65. Carazo E, Borrego-Sánchez A, Sánchez-Espejo R, García-Villén F, Cerezo P, Aguzzi C, et al. Kinetic and thermodynamic assessment on isoniazid/montmorillonite adsorption. Appl Clay Sci. 2018;165:82–90. https://doi.org/10.1016/j.clay.2018.08.009.

66. Cortesão AM, Henriques JG, Castro RAE, Maria TMR, Canotilho J, Eusébio MES. Binary phase diagrams of pyridinecarboxamide isomers. J Therm Anal Calorim. 2017;130:1727–33. https://doi.org/10.1007/s10973-017-6474-2.

67. Dengale SJ, Grohganz H, Rades T, Löbmann K. Recent advances in co-amorphous drug formulations. Adv Drug Deliv Rev. 2016;100:116–25. https://doi.org/10.1016/j.addr.2015.12.009.

68. Szabó-Révész P. Modifying the physicochemical properties of NSAIDs for nasal and pulmonary administration. Drug Discov Today Technol. 2018;27:87–93. https://doi.org/10.1016/j.ddtec.2018.03.002.

69. Kress HG, Baltov A, Basiński A, Berghea F, Castellsague J, Codreanu C, et al. Acute pain: a multifaceted challenge—the role of nimesulide. Curr Med Res Opin. 2016;32:23–36. https://doi.org/10.1185/03007995.2015.1100986.

70. Bendas ER, Abdelbary AA. Instantaneous enteric nano-encapsulation of omeprazole: pharmaceutical and pharmacological evaluation. Int J Pharm. 2014;468:97–104. https://doi.org/10.1016/j.ijpharm.2014.04.030.

71. Nogueira RC, Pinheiro LC, Sanches-Lopes JM, Parente JM, Oliveira-Paula GH, Conde SO, et al. Omeprazole induces vascular remodeling by mechanisms involving xanthine oxidoreductase and matrix metalloproteinase activation. Biochem Pharmacol. 2021;190: 114633. https://doi.org/10.1016/j.bcp.2021.114633.

72. Murakami FS, Lang KL, Mendes C, Cruz AP, Filho MASC, Silva MAS. Physico-chemical solid-state characterization of omeprazole sodium: thermal, spectroscopic and crystallinity studies. J Pharm Biomed Anal. 2009;49:72–80. https://doi.org/10.1016/j.jpba.2008.10.005.

73. Healy AM, Worku ZA, Kumar D, Madi AM. Pharmaceutical solvates, hydrates and amorphous forms: a special emphasis on cocrystals. Adv Drug Deliv Rev. 2017;117:25–46. https://doi.org/10.1016/j.addr.2017.03.002.

74. Essa EA, Elbasuony AR, Abdelaziz AE, El Maghraby GM. Co-crystallization for enhanced dissolution rate of bicalutamide: preparation and evaluation of rapidly disintegrating tablets. Drug Dev Ind Pharm. 2019;45:1215–23. https://doi.org/10.1080/03639045.2019.1571504.

75. Surov AO, Solanko KA, Bond AD, Bauer-Brandl A, Perlovich GL. Cocrystals of the antiandrogenic drug bicalutamide: Screening, crystal structures, formation thermodynamics and lattice energies. CrystEngComm R Soc Chem. 2016;18:4818–29. https://doi.org/10.1039/c6ce00931j.

76. Chavan RB, Thipparaboina R, Kumar D, Shastri NR. Co amorphous systems: a product development perspective. Int J Pharm. 2016;515:403–15. https://doi.org/10.1016/j.ijpharm.2016.10.043.

77. Banerjee M, Nimkar K, Naik S, Patravale V. Unlocking the potential of drug-drug cocrystals: a comprehensive review. J Control Release. 2022;348:456–69. https://doi.org/10.1016/j.jconrel.2022.06.003.